

ヒト大腸がん組織近傍の暗視野顕微観察像の偏光特性

藤井 透, 山崎康子, 齋藤直洋, 澤田正康, 成田 亮, 齋藤 拓, Heather L Durko, Photini Faith Rice, Gabrielle Vanessa Hutchens, Joceline Dominguez-Cooks, Harrison Taylor Thurgood, Swati Chandra, Valentine Nfonsam, Jennifer Kehlet Barton

Polarization characteristics of dark-field microscopic images of human colon tissue adjacent to tumor[†]

Toru FUJII, Yasuko YAMASAKI, Naooki SAITO, Masayasu SAWADA, Ryo NARITA, Taku SAITO, Heather L DURKO, Photini Faith RICE, Gabrielle Vanessa HUTCHENS, Joceline DOMINGUEZ-COOKS, Harrison Taylor THURGOOD, Swati CHANDRA, Valentine NFONSAM and Jennifer Kehlet BARTON

イメージング技術を用いたがんの早期検出は患者の生存率を大きく左右する。染色なしの従来の顕微画像に加え、共焦点顕微鏡、光干渉断層法、拡散反射分光法、などの情報を従来の医療光学画像に加えて使用し、in situ で早期癌を検出する多くの研究がなされている。豊富な偏光情報を有するミュラー偏光顕微測定を行い、組織による偏光変換のパラメーター空間の構造を調査するために、複数の照明波長で測定されたヒト大腸組織のミュラー行列成分を主成分分析した。またミュラー行列をコヒーレント行列にマッピングして分析し、固有値分析を行った。がん近傍領域の主成分分析を散布図表示した結果、非がん、非がんとがんの間、がん、の3つのタイプに別れ、がんタイプは第5主成分以降の量が正常値の3倍程度見られた。

Early detection of cancer through medical imaging has a critical impact on patient survival rates. There are many efforts for detecting early cancer in situ using advanced optical imaging. Unlike traditional medical optical imaging of biological tissues, which only provides information about surface morphology, these advanced modalities provide information on subsurface structure or function, without the need for staining, including confocal microscopy, optical coherence tomography, diffuse reflectance spectroscopy, and Mueller polarimetry. We analyzed Mueller matrix components of human colon tissue measured by imaging polarimeter microscope, at illumination wavelengths of 405, 442, 473, 543 and 632 nm, by principal components analysis in order to separate novel information from traditional non-polarized gray image and to investigate the structure of the parameter space of polarization transformation by tissue. We also analyzed Mueller matrix by mapping it to coherent matrix and performed eigenvalue analysis. 99% information exists from first to fourth principal components and polarization information is less than 10% of the total information of Mueller matrix. Scatter plotted principal components of the non-cancer tissue adjacent to the affected area visually categorized in three types of non-cancer, between noncancer and cancer, and cancer. Residues of the first to fourth principal components of the last type showed abnormality, whose value is three times larger than the noise level of the instrument used.

Key words 偏光, 主成分分析, ヒト大腸がん, 暗視野照明, ミュラー行列, コヒーレント行列, 固有値分析, エントロピー
polarization, principal component analysis, human colon cancer, dark-field illumination, Mueller matrix, coherent matrix, eigenvalue analysis, entropy

1 INTRODUCTION

Early detection of cancer through medical imaging has a critical impact on patient survival rates. Using traditional medical optical images of tissue, a convolutional neural net-

work (CNN) showed performance better than the expert specialist, as demonstrated by AlphaGo developed by Alphabet Inc.'s Google DeepMind. Recently, CNN has been shown to detect gastric cancer as accurately as an experienced endoscopist¹⁾. CNN must become a powerful tool with tradi-

[†] This paper was modified from Ref 21 and added a new result as chapter 4.

tional visible medical images, whose performance is as high as doctors.

There are many efforts for detecting early cancer for in situ usage using other modalities than the traditional images, which contain additional information other than conventional micrographs of surface morphology, without staining. Fast and minimally invasive optical techniques such as confocal microscopy²⁾ and optical coherence tomography (OCT)³⁾ are well-suited for producing detailed morphological characterizations of small (mm^2) samples.

Polarization interaction is used in diffuse reflectance spectroscopy⁴⁾ and Mueller polarimetry⁵⁾ imaging because polarimetry is sensitive to micro to nanometer structures as is explained by Mie scattering theory⁶⁾. Backman et al⁷⁾, present an optical-probe technique of based on light-scattering spectroscopy that is able to detect precancerous and early cancerous changes in cell-rich epithelia. They utilized the nature of early cancer cells which alter the epithelial-cell architecture in which the nuclei become enlarge. The diameter of non-dysplastic cell nuclei is typically 5–10 μm , whereas dysplastic nuclei can be as large as 20 μm across⁸⁾.

Intensive works concerning to Mueller matrix macro imaging of human colon tissue for cancer diagnostics with Mueller matrix decomposition to extract the essential polarimetric effects, namely the diattenuation, the retardation and the depolarization was done⁹⁾¹⁰⁾.

Polarization imaging with Monte Carlo simulations of backscattering Mueller matrix macro images of colon tissue were performed Novikova et al.¹¹⁾, who measured spectral Mueller matrix images of *ex vivo* human colon tissue and have shown with experiments and modeling that light scattering by small scatterers and light absorption are the key factors for observed polarimetric image contrast.

An imaging polarimeter microscope that operates in a backscattering configuration has been developed for usage of tissue classification and early cancer detection¹²⁾¹³⁾. The difference between the mean measured Mueller matrix values of healthy and cancerous human colon tissue agreed with previously reported results.

W. Wang et al.¹⁴⁾ measured histologically sliced sample Mueller matrix of the principal components analysis (PCA) derived from Mueller matrix elements for tissue differentiation.

In order to investigate polarization transformation dissect in pure components represented using Jones matrix and depolarization components induced by various human colon tissues, we analyzed 16 Mueller matrix components, measured by the imaging polarimeter microscope, by PCA. Each principal component was examined by comparing correlation

to non-polarized gray images, which includes traditional tissue morphological information used in CNN cancer detection. We also mapped Mueller matrix to coherent matrix and performed eigenvalue analysis.

2 PRINCIPAL COMPONENT ANALYSIS

Mueller matrix components of human colon tissues from 21 patients, measured using our imaging polarimeter microscope¹³⁾ with 5x objective and 442 nm (FWHM < 3 nm) illumination, were used in our analysis. There are three types of human colon tissues, Tumor, Adjacent taken apart from 5 mm from Tumor edge, and Normal from 50 mm apart from Tumor edge.

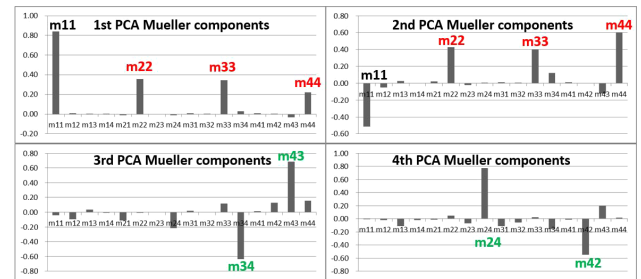


Fig. 1 Mueller matrix components of from first to fourth principal components of all 21 patients' tissues. Average vector of all images is 0.3 times of 1st PCA vector.

The imaging polarimeter system consists of an episcopic illumination system capable of dark-field illumination and a polarimetric imaging system for measuring the state of polarization (SOP) of scattered light from the tissue sample positioned at the microscope's specimen stage.

Figure 1 shows Mueller components of common PCA axes from 1st to 4th components analyzed by using 123 images of 21 patients. We also calculate PCA axes of each 123 images and found that 89.3 +/- 6.2% of the each 4-dimensional coordinate's space were found in the common PCA 4-dimensional space.

Figure 2 shows cumulative contribution rate principal

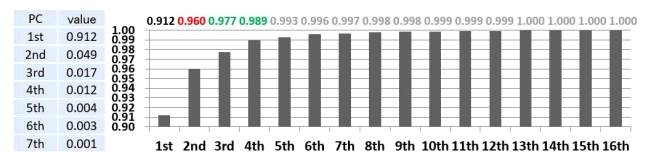


Fig. 2 Cumulative contribution rate principal components from 1st to 16th. Horizontal axis indicates number of cumulative components, in which components were added from 1st to N-th components. Vertical axis indicates value of cumulative components. A 4th cumulative component is 0.989.

components from 1st to 16th. Almost information of 99% is included from 1st to 4th PCA space.

When we treat these 4 matrices from 1st to 4th as Jones N-matrix¹⁵⁾, 1st to 4th axes correspond to scalar dissipation (extinction) i.e., attenuator (91.2% information), scalar depolarization (polarization extinction, 4.9% information), retardation difference between S1 and -S1 i.e., waveplate of S1 axis (1.7%), retardation difference between S2 and -S2 i.e., waveplate of S2 axis (1.2%). 5th and 6th (not shown in Fig. 1) correspond to transformation from S1 to S2 and S3 (0.4%), and transformation between S1 and S2 (0.3%).

Wang et al.¹⁴⁾ reported that significant differences in most

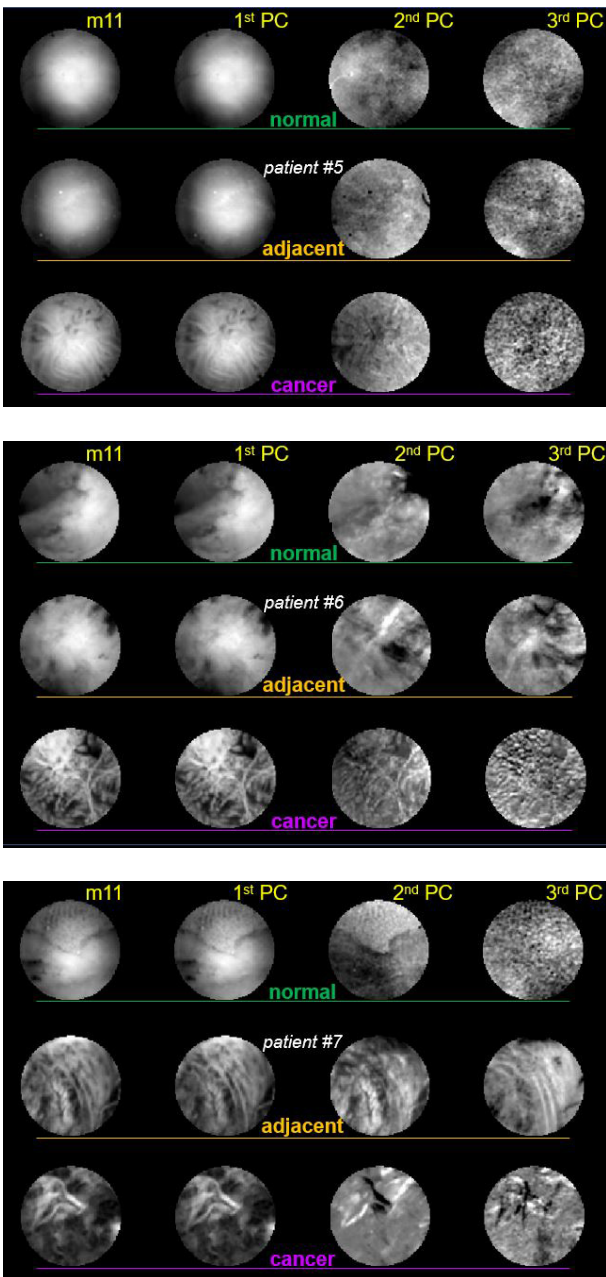


Fig. 3 m11, 1st to 3rd PCA score normal, adjacent and cancer images patient 5, 6 and 7. Field of view is 3.67 mm. Fine structures are not always related to each other.

parameters including retardance, depolarization, linear retardance, linear depolarization and circular depolarization between normal and cancer gastric samples and found that the combination of linear depolarization and linear retardance shows the best overall classification accuracy for gastric samples. In our case, for colon tissue, significant differences in polarization parameters were observed in the linear depolarization and linear retardance, which are the parameters for gastric cancer classification. The freedom of polarization parameter of colon might be slightly different from gastric of the stomach.

Figure 3 shows m11 and 3 principal component images. As discussed above, we can interpret each image corresponding to gray image, which is similar to m11 image, depolarization component image, wave plate component images. The perturbation of scalar intensity and scalar depolarization are seen in 1st and 2nd PCA score images, whose modulations are closely related each other. The trace of intensity remains in 3rd PCA score images as seen in patient 5 cancer images, when an image intensity modulation is large.

Fine structures observed in 2nd score and 3rd score have different information from 1st score image, which is assumed to be traditional images. This result confirmed the high rate existence of information in 3-dimensional PCA space and the high sensitivity of the instrument we used for investigating polarization interaction of human colon tissues with high special resolution. However, no significant differences in the images of the adjacent tissue could be observed.

3 EIGENVECTOR ANALYSIS AND ENTROPY

Mueller matrix M_{ij} can be mapped to coherent matrix C_{ij} by (1), η_k is Dirac matrix⁵⁾.

$$C = m_{ij} \eta_{4(i-1)+(j-1)}, 1 \leq i, j \leq 4, \eta_k, 0 \leq k \leq 15 \quad (1)$$

C_{ij} contains four eigenvectors, which correspond to 4 Jones matrices. Target entropy H_T is calculated by (2)¹⁴⁾¹⁵⁾.

$$H_T = -\sum_{i=1}^4 P_i \log_4 P_i \quad (2)$$

$$P_i = \frac{\alpha_i}{\sum_{j=1}^4 \alpha_j}$$

α_i : eigenvalue of C

There are several methods to quantify entropy, which are related to such as depolarization index¹⁶⁾, average degree of polarization¹⁷⁾, and several decomposition based methods^{18)~20)}. We used entropy because decomposed Jones matrix, which has the largest eigenvalue, can be used to

Table 1 Response of entropy against each patient with more precise diagnosis. Value of Site 1 and 2: Difference of mean entropy between tumor image pixels and normal image pixels (~5400 pixel each). Unit is a standard deviation of the each patient data. Higher number indicates that the tumor entropy is lower than that of normal, which means entropy response is positive and effective. Minus sign means tumor entropy is higher than normal one. We also analyzed images of patients 17 to 21, not shown in this table without precise clinical diagnosis nor pathology from hospital.

Patient No	Site1	Site2	Clinical Diagnosis	Pathology from hospital [a]	PCA type
1	4.7	4.4	right colon cecal mass	tubulovillous adenoma	N/A
2	0.1	0.7	sigmoid colon cancer	municous adenocarcinoma, low grade; T4aN1	normal
3	1.5	1.2	rectosigmoid colon mass	T4aN1a; focally invasive adenocarcinoma, moderately differentiated	normal
4	1.8	2.3	metastatic colon cancer	T3N1a adenocarcinoma	A on C
5	2.9	3.9	distal sigmoid colon adenocarcinoma staged as a T2N0M0 preop	well differentiated invasive adenocarcinoma arising from tubulovillous adenoma; pT1N1b	between
6	5.1	2.2	rectal mass	colonic mucosa fragments w/high-grade dysplasia concerning for invasive disease.	normal
7	3.6	3.0	rectal adenocarcinoma	ypT4bN0M1c; G2* moderately differentiated	A on C
8	2.9	-0.2	Cecal Mass	Tubulovillous adenoma	normal
9	0.2	0.0	Rectal cancer with a bowel obstruction	T3N2, invasive poorly differentiated adenocarcinoma	normal
10	0.5	2.3	Distal rectal polyp	Tubular adenoma	normal
11	2.3	4.3	Distal sigmoid colon cancer	pT3N0M0, Invasive adenocarcinoma, moderately to poorly differentiated, involving pericolonc adiposetissue	between
12	-1.2	-0.9	Ascending colon cancer	Sessile serrated adenoma with cytologic dysplasia	normal
13	2.4	2.9	Hepatic flexure adenocarcinoma		between
14	-1.9	-2.4	Rectal Cancer, patient 62 new mass, after chemoradiation	Invasive adenocarcinoma, T4bN1cM1c	normal
15	4.2	4.1	Sigmoid colon cancer	Medullary carcinoma, T4aN2b	between
16	-2.5	-3.5	Rectal cancer post chemotherapy	Moderately differentiated invasive adenocarcinoma, T3, N0	normal

[a] Staging index, Tumor (T): Tumor grown index, Node (N): Tumor spread index, Metastasis (M): Cancer metastasized index, *G2: the second subphase of interphases in the cell cycle directly preceding mitosis.

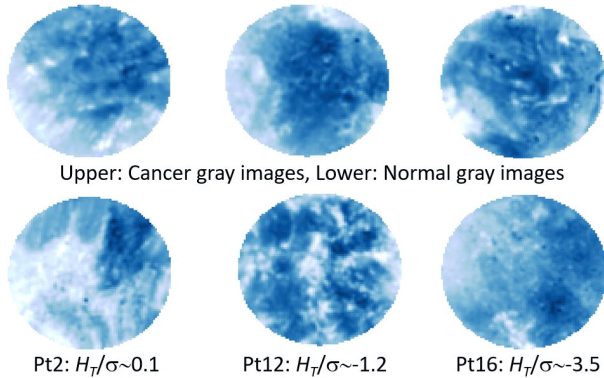


Fig. 4 Upper images: Gray scale traditional images of cancer, whose entropy is fairly lower than that of the normal images of the same patient. Lower images: Entropy images of the upper images. Field of view is 3.67 mm.

know optical characteristics when the largest eigenvalue is fairly larger than that of the rest ones.

Table 1 is an index that uses entropy and is shown in the columns of Site 1 and Site 2 and corresponding information of clinical diagnosis and Pathology from hospital. Totally analyzed sites i.e., images are 42 and 29 sites indicated lower entropy than that of normal site by the standard deviation of 5400 pixel data in each image. This result is well correlated

with 3-dimensional PCA projected result shown in figure 3 because 2nd PCA axis correlates to a direction of a degree of depolarization.

The largest discrepancy is seen in the patients who got chemoradiation and chemotherapy. Even there is a correlation between entropy and cancer, as was shown in Fig. 4, entropy responses, in some cases, also depend on the apparent morphology. This table also indicates that the current diagnosis is not simply related to entropy.

4 PRINCIPAL COMPONENT SCATTER DIAGRAM

Tissue adjacent to the affected part visually determined as cancer and visually determined as non-cancerous is of great interest as a research subject for dysplasia that transitions from normal tissue to early cancer. Figure 5 shows the example of distribution of the 1st and 2nd score principal component scatter diagram.

The distribution of the three types of tissue, as is indicated c: cancer, a: adjacent and n: normal in Fig. 5 on the scatter plot can be roughly divided into three patterns.

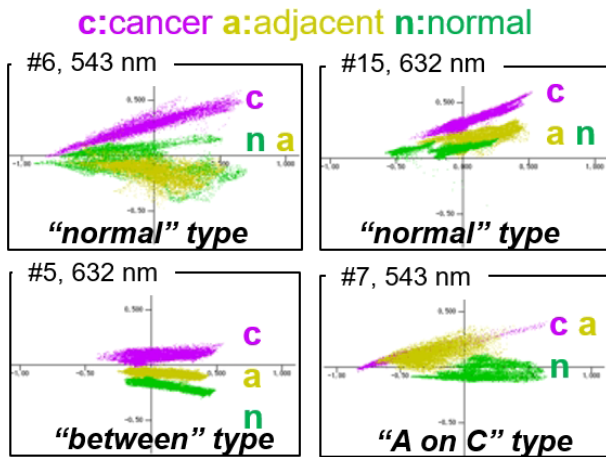


Fig. 5 1st and 2nd score principal component scatter diagram. Lateral and vertical axes are 1st and 2nd principal components, respectively. Each plotted region colored by purple, yellowish brown and green is cancer, adjacent and normal, respectively. “#” and nm indicates a patient number in table1 and illumination wavelength, respectively.

Which patterns belonged to each patient is shown in the rightmost column of Table 1. 1st pattern, called “normal” in Table1 shown in upper two scatter diagrams indicates distribution of the adjacent and the normal area overlap. The adjacent plots are located between the cancer and normal plots shown in #5, 623 nm plot as 2nd pattern, which is called “between” in table1. In the 3rd pattern called “A on C” of patient 7, which means adjacent is plotted on cancer region, the lower-right scatter plot in figure 5, the cancer and the transition region overlap. Residue of Mueller matrix 4 PCA components of patient 7 adjacent tissue is also three times larger than the noise level of the instrument used, as was reported in Ref. 23. Further investigation against adjacent tissue is expected to lead to early cancer detection.

5 CONCLUSION

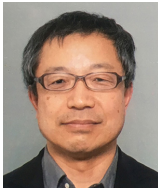
We analyzed 16 Mueller matrix components, measured by the imaging polarimeter microscope whose illumination wavelength was 442 nm, by PCA in order to separate from traditional non-polarized gray image and to investigate polarization interaction between human colon and illuminated light. Each principal component was examined by comparing between non-polarized gray images, which is traditional tissue morphological information used in CNN cancer detection. We also analyzed the Mueller matrix by mapping it to coherent matrix and performed eigenvalue analysis. 99% information of human colon tissue exists from first to fourth principal components space and polarization information exists from second and later, whose amount is less than 10%

of the total information of Mueller matrix. Optical interactions induced by each principal component from 1st to 4th are, scalar dissipation directly related to conventional image, scalar depolarization, and retarder of S1 and S2, respectively. Their percentages are 91.2, 4.9, 1.7, and 1.2. Microscopic fine structures observed in 3rd score and 4th score have different information from traditional gray images. There were several interesting examples in principal components scatter plot that non-cancer tissue adjacent to the affected area visually determined as cancer plotted between cancer and normal or on cancer. This result indicates that the relationship between 1st PCA image and 2nd PCA image, in other words, between intensity and depolarization effect, may be essential for very early development of human colon cancer. Further investigation against adjacent tissue will be performed.

References

- 1) Y. Sakai, S. Takemoto, K. Hori, M. Nishimura, H. Ikematsu, T. Yano and H. Yokota: “Automatic detection of early gastric cancer in endoscopic images using a transferring convolutional neural network”, *Conf. Proc IEEE Eng. Med Bio Soc.*, Jul., (2018), 4138–4141.
- 2) James Pawley, (Ed.): *Handbook of biological confocal microscopy*, (Springer US 2006).
- 3) J. G. Fujimoto, C. Pitris, S. A. Boppart and M. E. Brezinski: “Optical Coherence Tomography: An Emerging Technology for Biomedical Imaging and Optical Biopsy”, *Neoplasia*. Jan., 2(1-2) (2000), 9–25.
- 4) Z. Zonios, L. T. Perelman, V. Backman, R. Manoharan, M. Fitzmaurice, J. V. Dam and M. S. Feld: “Diffuse reflectance spectroscopy of human adenomatous colon polyps in vivo”, *Appl. Opt.*, **38** (31) (1999), 6628–6637.
- 5) D. H. Goldstein, *Polarized Light*, CRC Press, (2003).
- 6) V. V. Tuchin, L. Wang and D. A. Zimnyakov: *Optical Polarization in Biomedical Applications*, (Springer Science & Business Media 2006).
- 7) V. Backman, R. Gurjar, K. Badizadegan, L. Itzkan, R. R. Dasari, L. T. Perelman and M. S. Feld: “Polarized light scattering spectroscopy for quantitative measurement of epithelial cellular structures in situ”, *IEEE J. Sel. Top. Quantum Electron.*, **5** (1999), 1019.
- 8) V. Backman, M. B. Wallace, L. T. Perelman, J. T. Arendt, R. Gurjar, M. G. Mueller, Q. Zhang, G. Zonios, E. Kline, T. McGillican, S. Shapshay, T. Valdes., K. Badizadegan, J. M. Crawford, M. Fitzmaurice, S. Kabani, H. S. Levin, M. Seiler, R. R. Dasari, I. Itzkan, J. V. Dam and M. S. Feld: “Detection of preinvasive cancer cells”, *nature*, **406** (2000), 35.
- 9) S. Alali and A. Vitkin: “Polarized light imaging in biomedicine: emerging Mueller matrix methodologies for bulk tis-

- sue assessment", *J. Biomed. Opt.*, **20**(6) (2015), 061104.
- 10) V. V. Tuchin: "Polarized light interaction with tissues", *J. Biomed. Opt.*, **21**(7) (2016), 071114.
 - 11) T. Novikova, A. Pierangelo, S. Manhas, A. Benali, P. Validire, B. Gayet and A. De Martino: "The origins of polarimetric image contrast between healthy and cancerous human colon tissue", *Appl. Phys. Lett.*, **102** (2013), 241103.
 - 12) Z. Chen, Y. Yao, Y. Zhu and H. Ma: "A collinear backscattering Mueller matrix microscope for reflection Muller matrix imaging", *Proc. of SPIE*, **10489** (2018), 104890M-1.
 - 13) N. Saito, K. Sato, T. Fujii, H. L. Durko, G. L. Goldstein, A. H. Phillips, J. Dominguez-Cooks, G. V. Hutchens, H. T. Thurgood, P. F. Rice and J. K. Barton: "Multispectral Mueller matrix imaging dark-field microscope for biological sample observation", *Proc. SPIE*, **10890** (2019), 10890-46.
 - 14) W. Wang, L. G. Lim, S. Srivastava, J. B.-Y. So, A. Shabbir and Q. Liu: "Investigation on the potential of Mueller matrix imaging for digital staining", *J. Biophotonics*, **9** (4) (2016), 364.
 - 15) R. C. Jones: "A new calculus for the treatment of optical systems. VII. Properties of the N-matrices," *J. Opt. Soc. Am.*, **38** (1948), 671-685.
 - 16) S. R. Claude and E. Pottier: "An Entropy Based Classification Scheme for Land Applications of Polarimetric SAR", *IEEE Transactions on Geoscience and Remote Sensing*, **35** (1997), 68-78.
 - 17) S. R. Claude: "Polarimetry: The characterization of polarization effects in EM scattering", Dr. Thesis University of Birmingham, (1987).
 - 18) J. J. Gil and E. Bernabeu: "Depolarization and polarization indices of an optical system" *OPTICA ACTA*, **33** (1986), 185-189.
 - 19) R. A. Chipman: "Depolarization index and the average degree of polarization", *Appl. Opt.*, **44**(13) (2005), 2490.
 - 20) S-Y. Lu and R. A. Chipman: "Interpretation of Mueller matrices based on polar decomposition", *JOSAA*, **13**(5) (1996), 1106.
 - 21) T. Fujii, Y. Yamasaki, N. Saito, M. Sawada, R. Narita, T. Saito, H. L. Durko, P. F. Rice, G. V. Hutchens, J. Dominguez-Cooks, H. T. Thurgood, S. Chandra, V. N. Nfonsam and J. K. Barton: "Polarization characteristics of dark-field microscopic polarimetric images of human colon tissue," *Label-free Biomedical Imaging and Sensing (LBIS)*, *Proc SPIE*, **10890** (2019), 108902J.



藤井 透
Toru FUJII
研究開発本部
光技術研究所
Optical Research Laboratory
Research & Development Division



Photini Faith RICE
The University of Arizona



山崎康子
Yasuko YAMASAKI
研究開発本部
光技術研究所
Optical Research Laboratory
Research & Development Division



Gabrielle Vanessa HUTCHENS
The University of Arizona



齋藤直洋
Naooki SAITO
研究開発本部
光技術研究所
Optical Research Laboratory
Research & Development Division



Joceline DOMINGUEZ-COOKS
The University of Arizona



澤田正康
Masayasu SAWADA
株式会社ニコンシステム
Nikon System Inc.



Harrison Taylor THURGOOD
The University of Arizona



成田 亮
Ryo NARITA
株式会社ニコンシステム
Nikon System Inc.



Swati CHANDRA
The University of Arizona



齋藤 拓
Taku SAITO
株式会社ニコンシステム
Nikon System Inc.



Valentine NFONSAM
The University of Arizona



Heather L DURKO
Nikon Research Corporation America



Jennifer Kehlet BARTON
The University of Arizona